On the Development of a Dense Optical Flow Benchmark Dataset for Satellite Meteorology Applications

Jason Apke[1] , *Kris Bedka*[2], *Matt Rogers*[1] *and Steven Miller*[1]

[1] *Cooperative Institute for Research in the Atmosphere (CIRA), Fort Collins, CO*

[2] *NASA Langley Research Center, Hampton, Virginia*

What is Dense Optical Flow?

- **Optical Flow Definition:**

  “The distribution of apparent velocities of movement of brightness patterns in an image” (Horn and Schunck 1981)

- “Dense” optical flow (DOF) is motion retrieval at EVERY image pixel
  - Contrast w/ sparse optical flow, where motion is tracked at specific targets in the image (e.g. AMVs; Velden et al. 1997; Bresky et al. 2012)
- Routine rapid scanning (≤ 5 min) now enables new and advanced DOF retrieval techniques for most cloud-motions in geostationary satellite imagery, and there are numerous applications

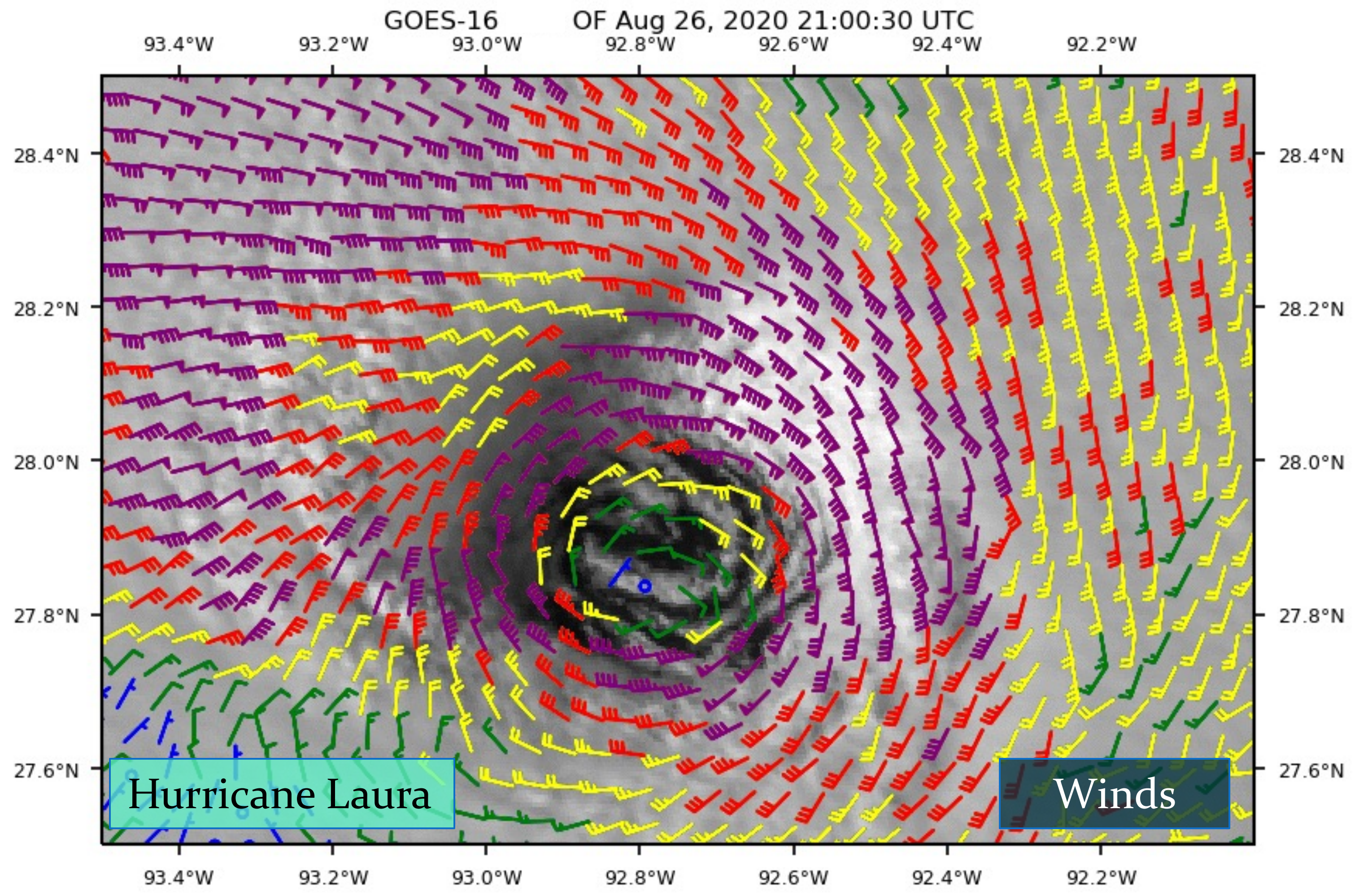

Figure 1. GOES-16 Ch-02 0.64 µm imagery plotted with Farnebäck optical flow (wind barbs colored by speed) over Hurricane Laura in the Gulf of Mexico.

Optical Flow Benchmarks

- Benchmarks are validation and training datasets designed to quantify progress and uncertainty in algorithm development
- Three Examples are Middlebury, MPI-Sintel, and KITTI
- Benchmarks ensure optical flow quality, and provide challenging tracking scenes to drive research forward

KITTI

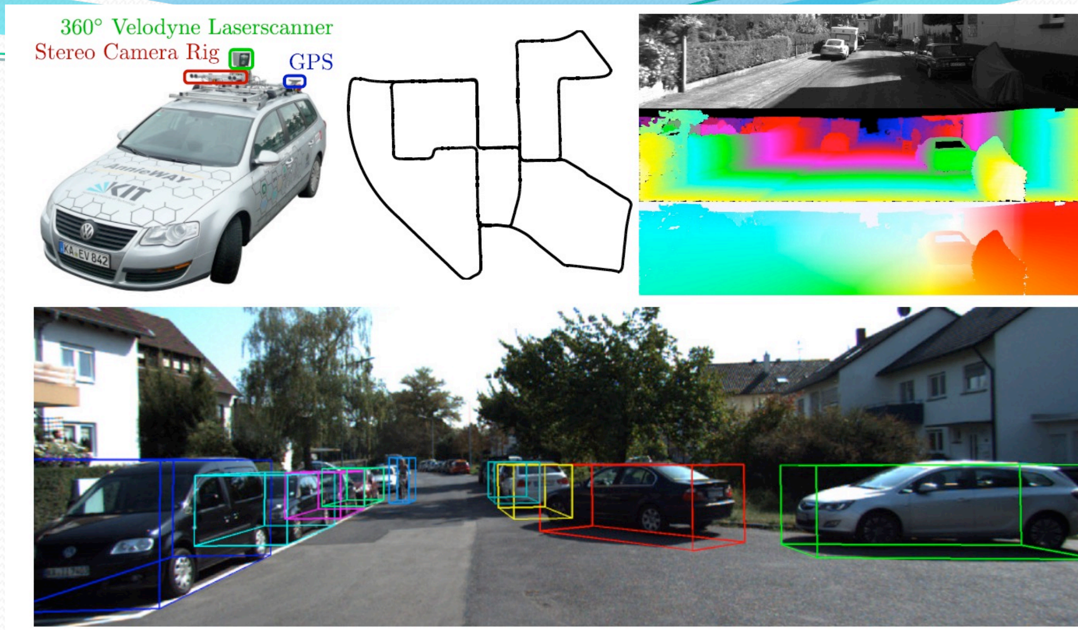

Middlebury “Army” Sequence

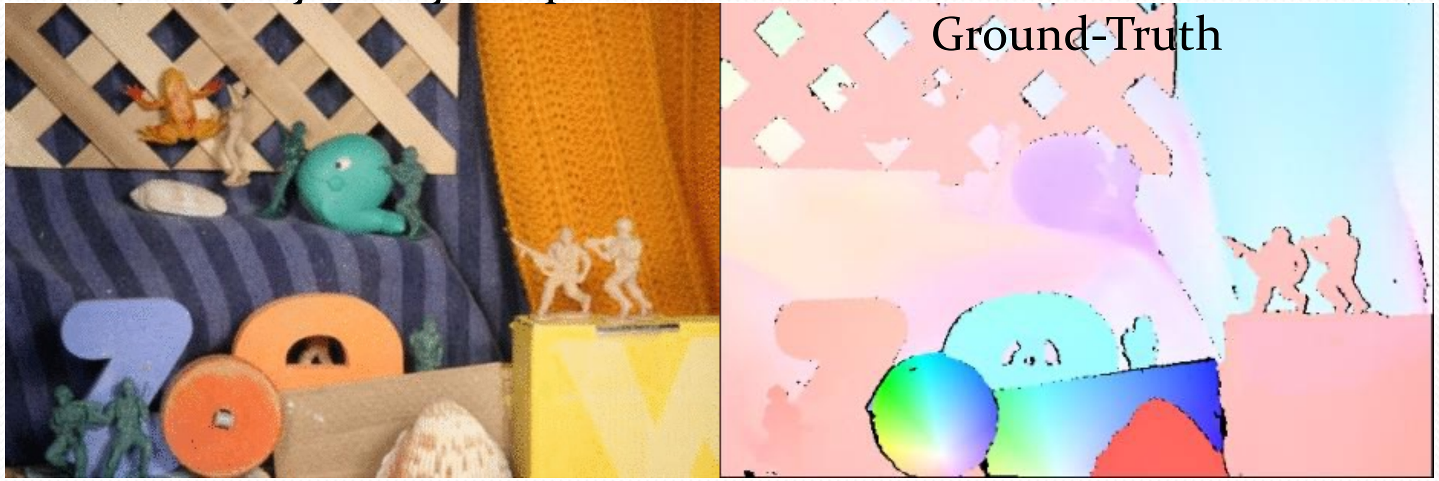

Baker, S., D. Scharstein, J. P. Lewis, S. Roth, M. J. Black, and R. Szeliski, 2011: A database and evaluation methodology for optical flow. *Int. J. Comput. Vis.*, **92**, 1–31, doi:10.1007/s11263-010-0390-2.

Butler, D. J., J. Wulff, G. B. Stanley, and M. J. Black, 2012: A naturalistic open source movie for optical flow evaluation. *Lect. Notes Comput. Sci. (including Subser. Lect. Notes Artif. Intell. Lect. Notes Bioinformatics)*, **7577 LNCS**, 611–625, doi:10.1007/978-3-642-33783-3_44.

Geiger, A., P. Lenz, and R. Urtasun, 2012: Are we ready for autonomous driving? the KITTI vision benchmark suite. *Proc. IEEE Comput. Soc. Conf. Comput. Vis. Pattern Recognit.*, 3354–3361, doi:10.1109/CVPR.2012.6248074.

Motivation

- The quality of DOF applications (Like AMVs) depend on *accurate* retrieval
- Most DOF algorithms were designed to track large, "quasi-rigid" scenes
  - Obstacle detection for self-driving cars (Fortun et al. 2016)
  - Automated Surveillance of moving pedestrians (e.g. Ring Doorbells)
  - Feature or Gesture Tracking (For virtual/augmented reality)
- The fluid motions in satellite imagery are a different tracking problem than what ordinary DOF validation datasets focus on
- DOF validation datasets can be used to
  1. Set benchmarks that result in measurable DOF development progress
  2. Help to identify strengths/weaknesses of different DOF retrieval techniques
  3. Inform on instrument design and scanning strategies (e.g. temporal /radiometric resolutions) for future satellite missions

Optical Flow Validation Methods

1) Validation with Wind Measurements (We use the Aeolus CAL/VAL DAWN data w/ GOES-17 1-min imagery; Bedka et al. 2020 *in review;* Validation includes Bias/Mean Vector Difference; MVD)
   - In many applications, it is assumed that optical flow = winds
   - Winds can be validated with in situ measurements (rawinsondes) or remote sensing tools (e.g. Doppler Radar/Lidar) wind profilers nearby in space/time
   - Key disadvantage: Not all brightness features move w/ the wind motion
     - E.G. gravity waves, surface features, outflow boundaries
2) Validation with Image Interpolation (We use Hurricane Michael 30-sec 0.64-µm GOES-16 imagery from 1700-1830 UTC; Following interpolation approach in Baker et al. 2011)
   - In many other applications, it may be beneficial to better track features
   - Optical Flow estimates can be combined with a simple interpolation algorithm to estimate intermediate frames and evaluate feature tracking performance
     - Performance is determined by comparing estimated image to a known image typically with a gradient normalized sum-of-square error
     - In most cases, this can be done w/ 1-min and 30-sec mesoscale sectors

Citation: Bedka, K. M and Co-Authors, 2020: Airborne Lidar Observations of Wind, Water Vapor, and Aerosol Profiles During The NASA Aeolus Cal/Val Test Flight Campaign [Preprint]. *Atmos. Mea. Tech., In Review.* https://doi.org/10.5194/amt-2020-475

Sun Et Al. (2014) Optical Flow

- New optical flow methods do handle motion discontinuities, illumination changes, and large displacements, Brox et al. (2004) for example minimizes this with a coarse-to-fine strategy:

$$E(u(\boldsymbol{x}), v(\boldsymbol{x})) = \iint_{\Omega} \rho_d(BC + \gamma\, GC) + \alpha\, \rho_s(SC) d\boldsymbol{x}$$

BC = Brightness Constancy -> $|I(\boldsymbol{x} + \boldsymbol{U}, t + \Delta t) - I(\boldsymbol{x}, t)|^2$

GC = Gradient Constancy -> $|\nabla I(\boldsymbol{x} + \boldsymbol{U}, t + \Delta t) - \nabla I(\boldsymbol{x}, t)|^2$, γ = weight of GC

Mitigates motion caused by illumination changes

SC = Smoothness Constraint -> $|\nabla u|^2 + |\nabla v|^2$, α = weight of SC

The $\rho_d(x^2) = \rho_s(x^2) = \sqrt{x^2 + \varepsilon^2}$ are "Robust Functions"

Preserves motion discontinuities in image field

- We will use a method by Sun et al. (2014), minimizing:

$$E_{Sun}(u, v, \hat{u}, \hat{v}) = E(u, v) + \lambda_c(\|\boldsymbol{u} - \hat{\boldsymbol{u}}\|^2 + \|\boldsymbol{v} - \hat{\boldsymbol{v}}\|^2) + \lambda_n \sum_{i,j} \sum_{(i',j') \epsilon N_{i,j}} w_{i\,j}^{i'j'} \left(|\hat{u}_{i\,j} - \hat{u}_{i'\,j'}| + |\hat{v}_{i\,j} - \hat{v}_{i'\,j'}|\right)$$

Brox Equation

Coupling Term (penalizes deviations from auxiliary field $\hat{\boldsymbol{u}}$, $\hat{\boldsymbol{v}}$)

Weighted Median Smoothing Term (within a neighborhood of $N_{i,j}$)

$$w_{i\,j}^{i'j'} = e\,\hat{}\left\{-\frac{|i - i'|^2 + |j - j'|^2}{2\sigma_1^2} - \frac{|I_{i,j} - I_{i'j'}|^2}{2\sigma_2^2}\right\}$$

- This better resolves motion discontinuities
- Has aux. flow field which we can set to known values
- Weighted median can be based on GOES-R fields

Winds Validation Results

- Optical flow validated by channel, for all case studies, fine-spatial resolution red-band (CH-2) validated the best, short-wave IR (CH-7) the worst
- Validation statistics here are comparable to recent validations of the Derived Motion Wind algorithm
- Sum-of-square-error tracking performs worse than the dense-optical flow algorithms here (NOTE: NO AMV QUALITY CONTROL PERFORMED HERE)

Table 2. Comparison statistics of CIRA/Sun optical flow algorithm and the Sum-Of-Square-Error Minimization to the DAWN lidar wind.

Case Study	Bias (Sun | SOSE ; m s^{-1})	MVD (Sun | SOSE ; m s^{-1})	Samples
April 17-18	-0.86 | -0.13	2.56 | 3.78	31
April 22-23	-0.48 | -0.81	1.68 | 3.78	208
April 25-26	-0.27 | 0.32	1.55 | 2.81	365
April 27-28	-0.31 | -0.09	3.32 | 5.62	582
April 29-30	-0.25 | 0.751	2.18 | 7.14	679
Total	-0.306 | 0.100	2.36 | 5.38	1865

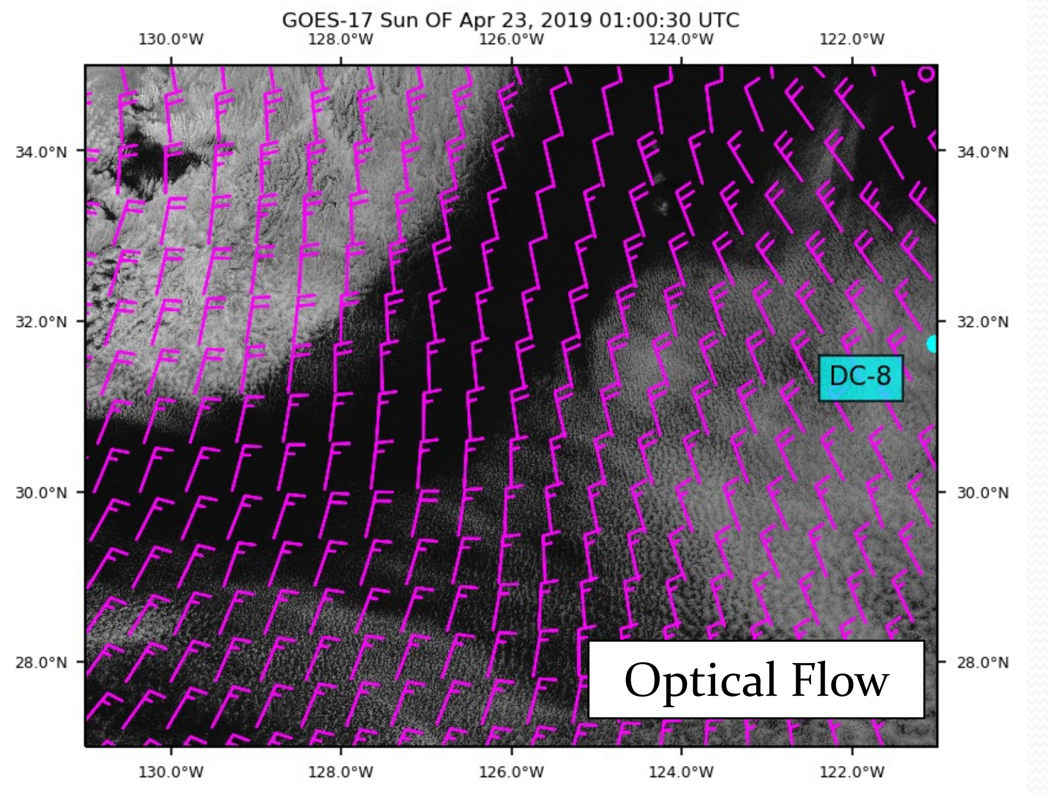

Figure 2. GOES-17 Ch-02 0.64 μm imagery plotted with Sun optical flow, along with the NASA-DC-8 location carrying the DAWN Lidar used for the ground-truth winds in the table on the left.

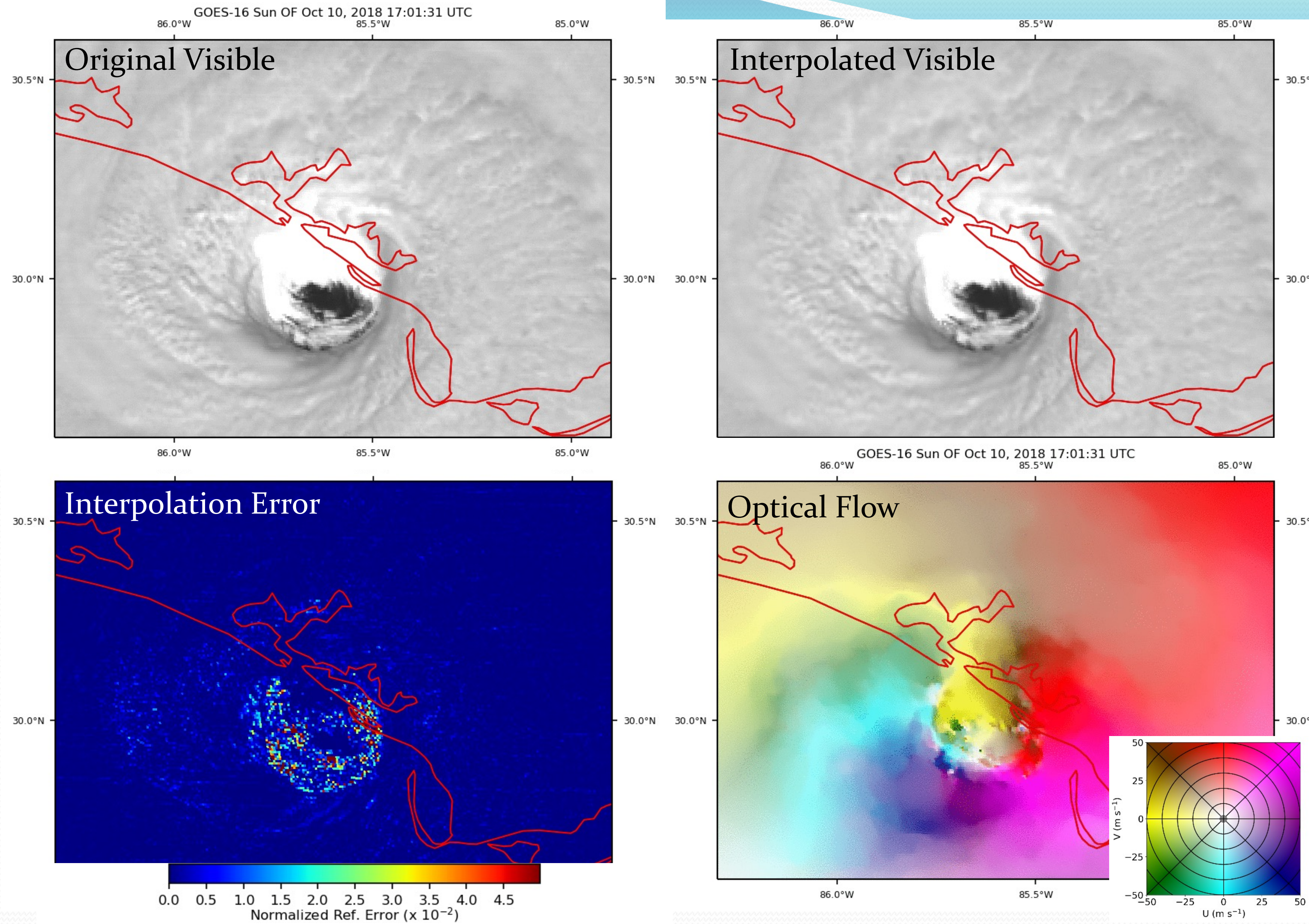

- CIRA-SUN method slightly outperforms Farnebäck
- Non-linear/ Occluding motions give DOF algorithms problems

GNSSE
Farneback = **0.0293**
CIRA Sun =**0.0286**

In Summary…

- A validation dataset is being developed for new dense-optical flow algorithms specifically for satellite meteorology datasets/applications (includes both winds and image interpolation-based validation)
- 6 cases were demonstrated (5 for winds/one with interpolation)
- Thus far, the CIRA-SUN optical flow method is outperforming sum-of-square error minimization for tracking clouds in the validation dataset (MVD ~ 2 m s^{-1} for visible imagery)
- CIRA-SUN Test interpolation does slightly better than open-source optical flow methods (and more work is underway to improve optical flow datasets using satellite data not available from typical imagers)
- DAWN Data DOI: 10.5067/AIRBORNE/AEOLUS-CALVAL-DAWN_DC8_1

Future Work

- Seeking to establish an open-source framework for benchmark delivery
    - Will include current statistics of cutting-edge optical flow techniques
    - Will be designed with data/code sharing in mind
- The benchmark is planned to include a set of optical flow challenges common in satellite remote sensing
    - Scenes containing motions that are transparent, texture-less, fast moving, deforming, propagating vs. advecting, convective vs. stratiform, clouds vs. snow/ice, dust vs. ground, small targets/boundaries edges (Any new suggestions are welcome!)
- Supplement winds validations with synthetic IR/WV imagery examples
- As many OF techniques today are Machine-Learning-based, we will also seek to establish training datasets for all to use

Acknowledgements

- Work was funded under NESDIS GOES-R Program Office award number: NA14OAR4320125 and NOAA Grant NA19OAR4320073.

Citations

Apke, J. M., J. R. Mecikalski, and C. P. Jewett, 2016: Analysis of Mesoscale Atmospheric Flows above Mature Deep Convection Using Super Rapid Scan Geostationary Satellite Data. *J. Appl. Meteorol. Climatol.*, **55**, 1859–1887, doi:10.1175/JAMC-D-15-0253.1. http://journals.ametsoc.org/doi/10.1175/JAMC-D-15-0253.1.

——, ——, K. M. Bedka, E. W. McCaul Jr., C. R. Homeyer, and C. P. Jewett, 2018: Relationships Between Deep Convection Updraft Characteristics and Satellite Based Super Rapid Scan Mesoscale Atmospheric Motion Vector Derived Flow. *Mon. Wea. Rev.*, **146**, 3461–3480. https://doi.org/10.1175/MWR-D-18-0119.1.

Brox, T., A. Bruhn, N. Papenberg, and J. Weickert, 2004: High accuracy optical flow estimation based on a theory for warping. *2004 Eur. Conf. Comput. Vis.*, **4**, 25–36.

Farnebäck, G., 2001: Two-Frame Motion Estimation Based on Polynomial Expansion. *Proceedings: Eighth IEEE International Conference on Computer Vision*, Vol. 1 of, 171–177.

Fortun, D., P. Bouthemy, C. Kervrann, D. Fortun, P. Bouthemy, and C. Kervrann, 2015: Optical flow modeling and computation : a survey To cite this version : Optical flow modeling and computation : a survey. *Comput. Vis. Image Underst.*, **134**, 1–21. https://hal.inria.fr/hal-01104081/file/CVIU_survey.pdf.

Horn, B. K. P., and B. G. Schunck, 1981: Determining optical flow. *Artif. Intell.*, **17**, 185–203, doi:10.1016/0004-3702(81)90024-2.

Sun, D., S. Roth, and M. J. Black, 2014: A quantitative analysis of current practices in optical flow estimation and the principles behind them. *Int. J. Comput. Vis.*, **106**, 115–137, doi:10.1007/s11263-013-0644-x.

Wu, Q., H.-Q. Wang, Y.-J. Lin, Y.-Z. Zhuang, and Y. Zhang, 2016: Deriving AMVs from Geostationary Satellite Images Using Optical Flow Algorithm Based on Polynomial Expansion. *J. Atmos. Ocean. Technol.*, **33**, 1727–1747, doi:10.1175/JTECH-D-16-0013.1. http://journals.ametsoc.org/doi/10.1175/JTECH-D-16-0013.1.

Thank You For Listening!

For additional questions, contact:

Jason Apke

jason.apke@colostate.edu

3925A West Laporte Ave. Fort Collins, CO 80523-1375

DAWN Data DOI: 10.5067/AIRBORNE/AEOLUS-CALVAL-DAWN_DC8_1

Connecting Models and Observations

Extra Slides

For additional questions, contact:

Jason Apke

jason.apke@colostate.edu

3925A West Laporte Ave. Fort Collins, CO 80523-1375

DAWN Data DOI: 10.5067/AIRBORNE/AEOLUS-CALVAL-DAWN_DC8_1

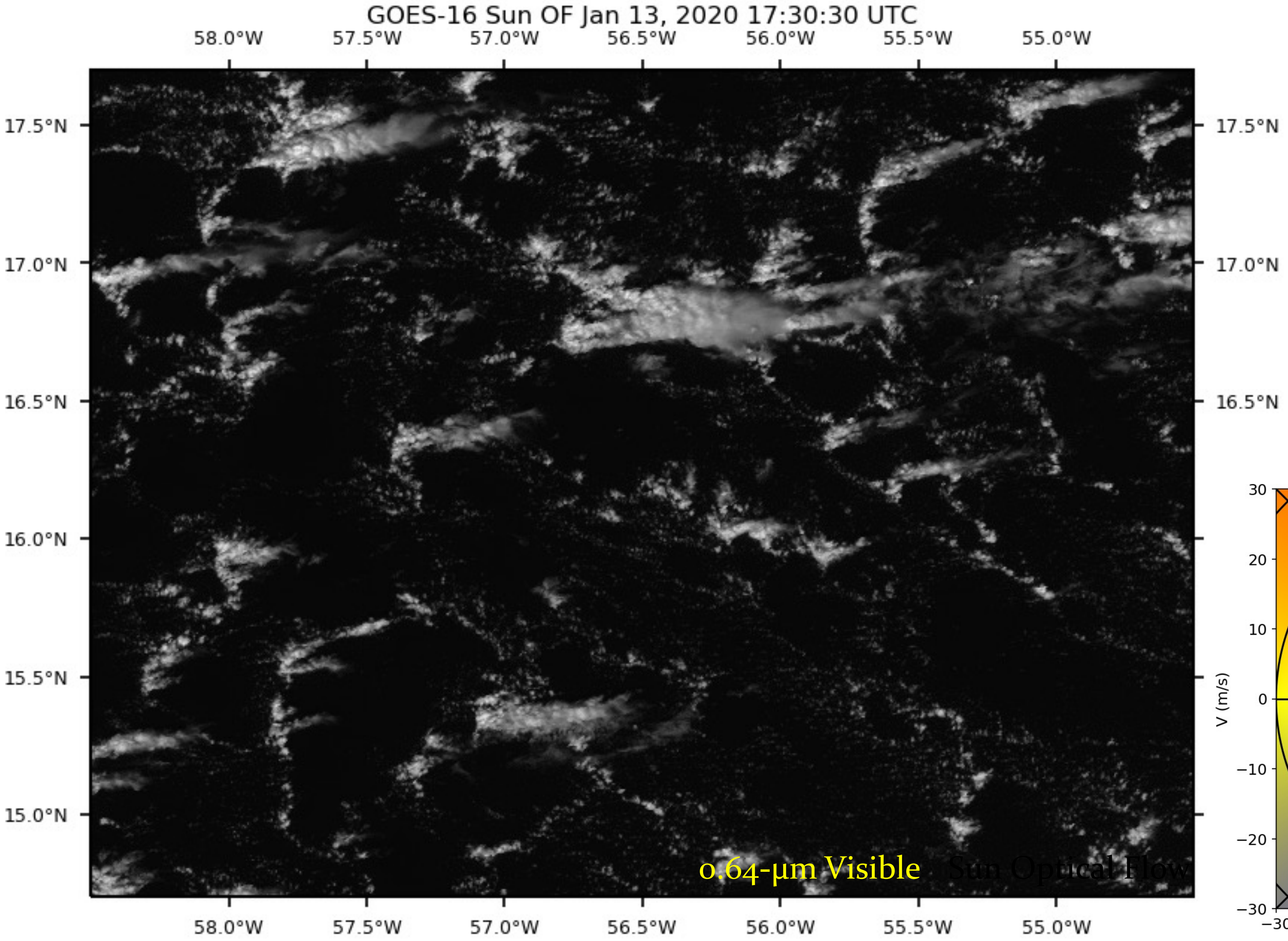

- Dense optical flow meso-winds products see vertical growth in clouds as acceleration in cloud-top horizontal motion, see color scale below (where grey=stationary)
- Hodograph (below) indicates GFS analysis wind speed and direction as a function of height for this scene

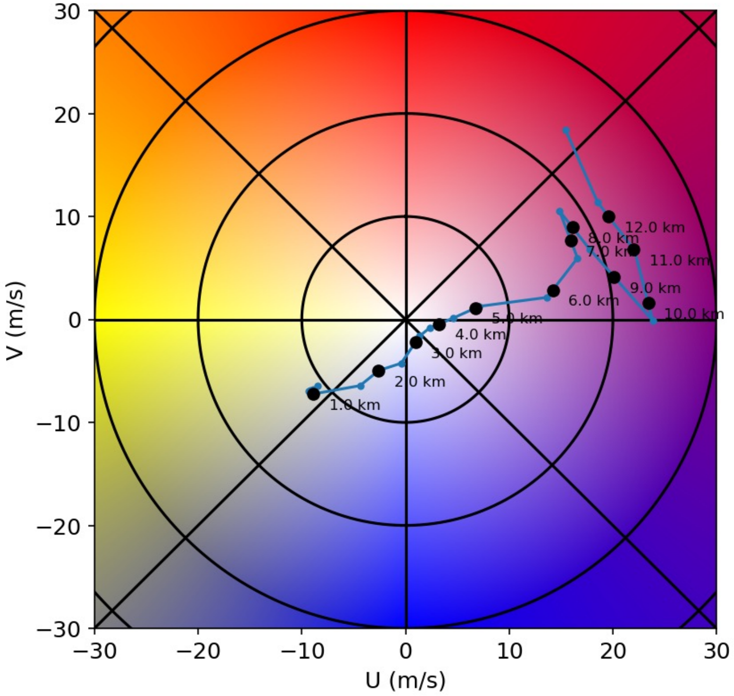

Cloud-Top Cooling

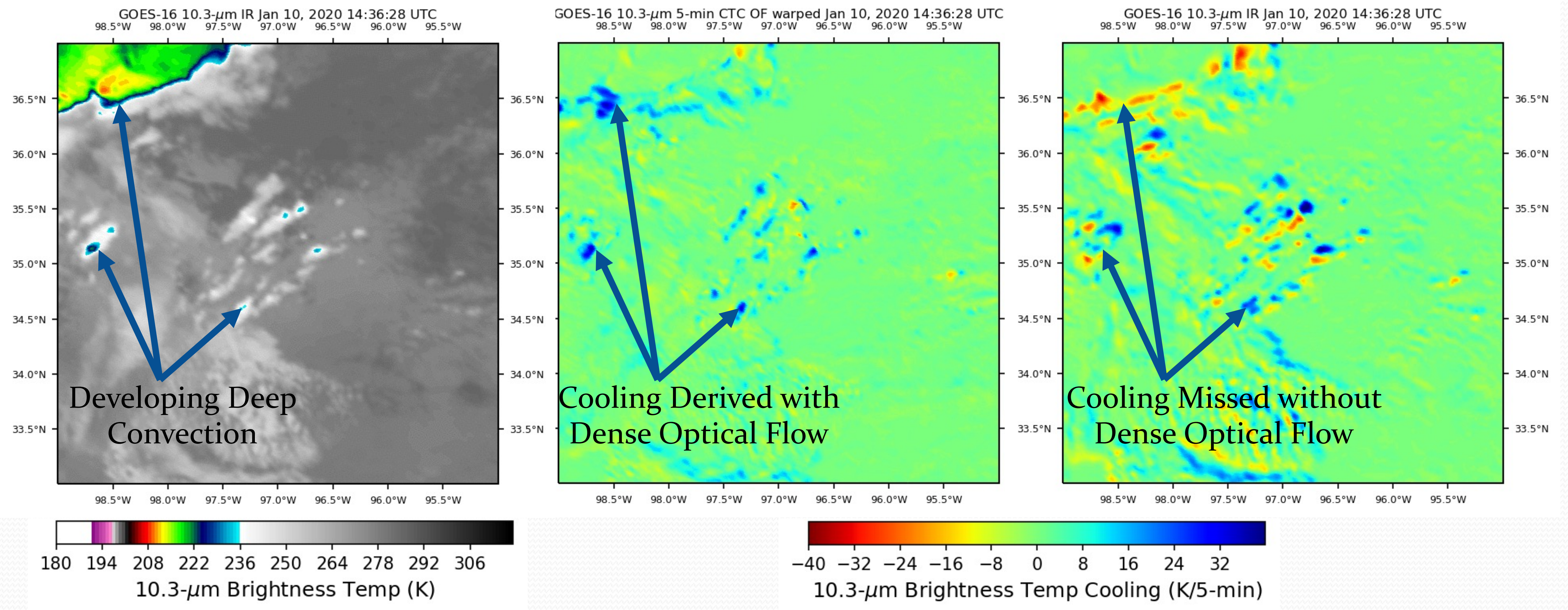

*Time-rates of change can *dramatically* complement the native 16-channels on GOES-R ABIs for AI/Machine Learning

DNB Imagery

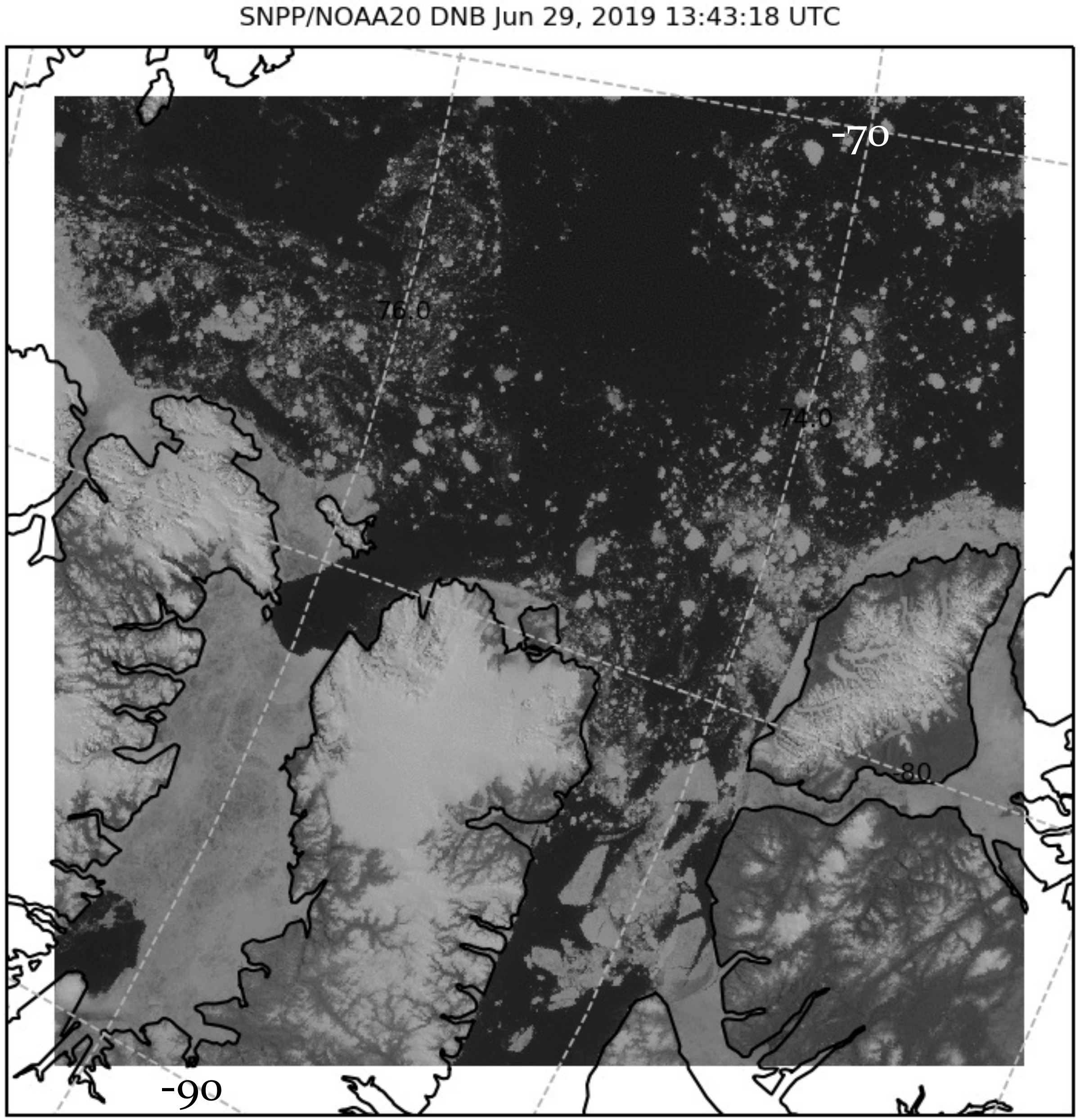

Color-Shaded Optical Flow Comparison

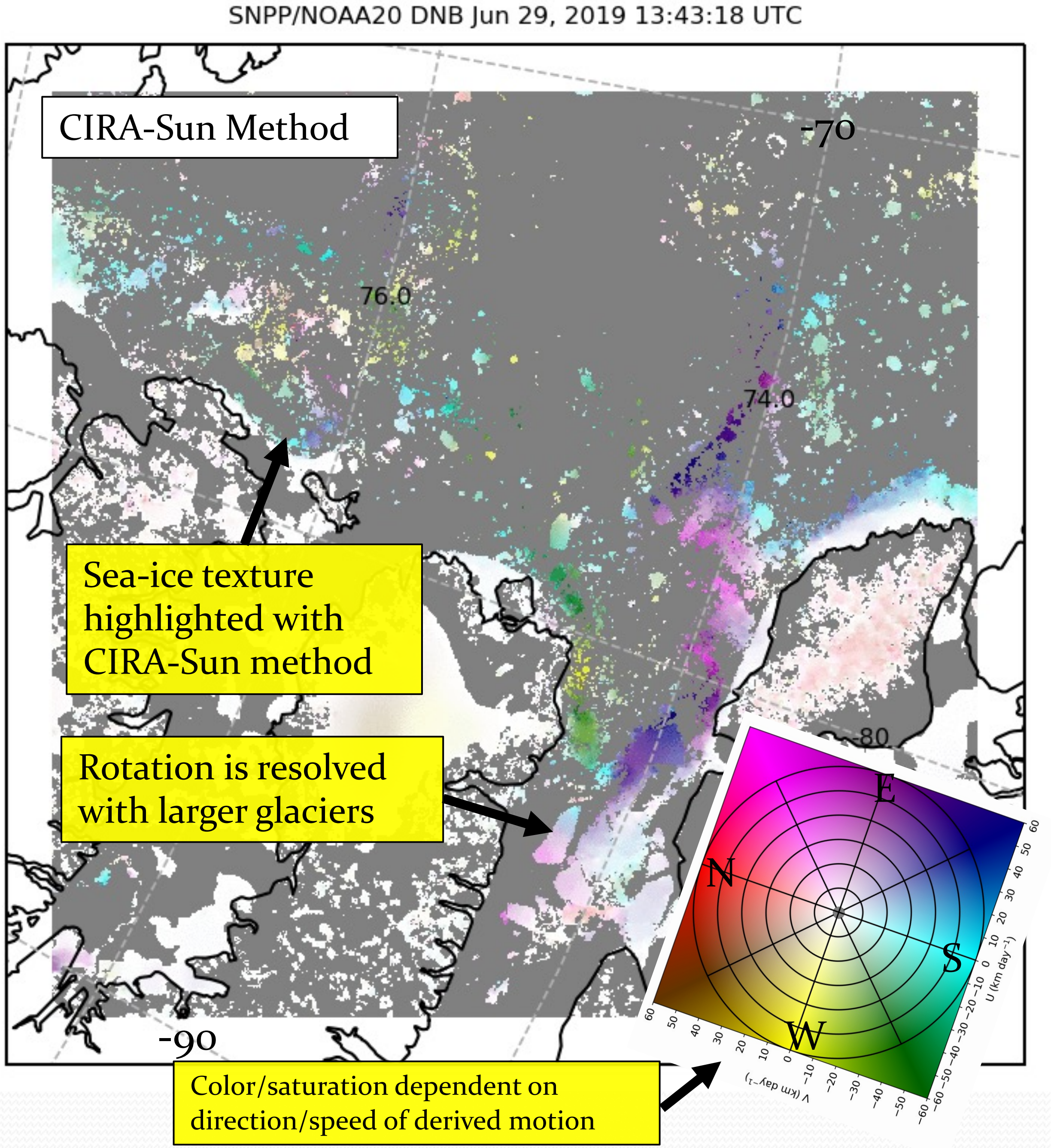

Winds Validation

- Two optical flow retrieval systems are run on 1-min GOES-17 images:
  - Sun et al. (2014), and a sum-of-square error minimization technique (following AMV methods; 5x5 pixel target box sizes; 9x9 search regions)
- Algorithm output is compared to NASA Aeolus Cal/Val aircraft field campaign data (Bedka et al. 2020)
  - Five DC-8 research flights over a two-week period in Spring, 2019
  - DC-8 carried the Doppler Aerosol Wind Profiling Lidar (DAWN; outputs winds and signal-to-noise ratio, SNR) under a GOES-17 1-min meso-sector
  - Assuming highest altitude SNR=10 value is the cloud-top wind derived by the optical flow approaches
  - We test winds by Bias and Mean Vector Difference (MVD)

$$Bias = \frac{1}{n}\sum \sqrt{u_{of}^2 + v_{of}^2} - \sqrt{u_{DAWN}^2 + v_{DAWN}^2}$$

$$MVD = \frac{1}{n}\sum \sqrt{(u_{of} - u_{DAWN})^2 + (v_{of} - v_{DAWN})^2}$$

Interpolation Validation

Connecting Models and Observations

- We test two optical flow algorithms with interpolation error, Sun et al. (2014) and an open source method by Farneback (2001)
- Optical Flow Interpolation follows Baker et al. (2011)
  - Inputs: Two sequential images, forward calculated (time 1 -> time 2) optical flow, intermediate time for new frame (in our case, $t = 0.5$), Interpolation is a four-step process:

1. Warp optical flow forward to the time to be interpolated, so $\boldsymbol{u_w}(round(\boldsymbol{x} + t\,\boldsymbol{u_0}(\boldsymbol{x})) = \boldsymbol{u_0}(\boldsymbol{x})$
2. Fill in any holes on the warped optical flow field with an outside-in strategy
3. Estimate Occlusion Masks (where only one image is visible at one time) using forward flow reasoning
4. Where both pixels are visible, blend the two images using $I_t(\boldsymbol{x}) = (1-t)I_0(\boldsymbol{x_0}) + t\,I_1(\boldsymbol{x_1})$ where I is the image brightness, $\boldsymbol{x_0} = \boldsymbol{x} - t\,\boldsymbol{u_w}(\boldsymbol{x})$, $\boldsymbol{x_1} = \boldsymbol{x} + (1-t)\,\boldsymbol{u_w}(\boldsymbol{x})$, t is the time between each image normalized such that the total time difference = 1,

   otherwise set pixel to forward/backward warped image which is not occluded

- Optical flow is run with 1-min cadence on 30-sec visible imagery, interpolated 30-sec image is then compared to the actual image w/ the gradient-normalized sum-of-square error,

$$GNSSE = \left(\frac{1}{n}\sum\frac{\left(I(x,y) - I_t(x,y)\right)^2}{\nabla I(x,y) + 0.1}\right)^{\frac{1}{2}}$$

Citation: Baker, S., D. Scharstein, J. P. Lewis, S. Roth, M. J. Black, and R. Szeliski, 2011: A database and evaluation methodology for optical flow. *Int. J. Comput. Vis.*, **92**, 1–31, doi:10.1007/s11263-010-0390-2.

Farnebäck Optical Flow

- Here, a scheme similar to Farnebäck (2001) and Wu et al. (2016) is used
  - Identifies flow by fitting image intensity I in windows to polynomial functions, that is:

$$I(\boldsymbol{x}) = \boldsymbol{x}^T \boldsymbol{A}\, \boldsymbol{x} + \boldsymbol{B}\, \boldsymbol{x} + \boldsymbol{C}$$

  - Where I is a function of the position in the image window **x**=[x,y] and constant coefficient matrices $\boldsymbol{A}$, $\boldsymbol{B}$ and $\boldsymbol{C}$
  - With linear algebra, the coefficients of the polynomial in two subsequent image windows can be used to solve for the flow **u** assuming brightness constancy, that is, at time t+1

$$I(\boldsymbol{x}, t) = I(\boldsymbol{x} + \boldsymbol{u}, t + 1)$$

And it can be shown that

$$\boldsymbol{u} = -\frac{1}{2}\boldsymbol{A}_1^{-1}(\boldsymbol{B}_2 - \boldsymbol{B}_1)$$

* Note: $\boldsymbol{u}$ cannot be found $\boldsymbol{A}_1$ if is not invertible (e.g. when there is no texture)!

- OpenCV (opencv.org) Farnebäck function used with the following settings
  - Window: 5 x 5 pixels, local optimization window: 25x25 pixels
  - Pyramid Depth- 3 levels, Scaling- 0.5
  - Smoothing Std. Dev.- 1.0, Farnebäck Gaussian Smoothing Used
  - Sets $\boldsymbol{u} = [0,0]$ when no texture is available to find a solution!

Citation: Wu, Q., H.-Q. Wang, Y.-J. Lin, Y.-Z. Zhuang, and Y. Zhang, 2016: Deriving AMVs from Geostationary Satellite Images Using Optical Flow Algorithm Based on Polynomial Expansion. *J. Atmos. Ocean. Technol.*, **33**, 1727–1747, doi:10.1175/JTECH-D-16-0013.1.

Doppler Aerosol Wind (DAWN) Lidar System

PI: Michael J. Kavaya, NASA LaRC

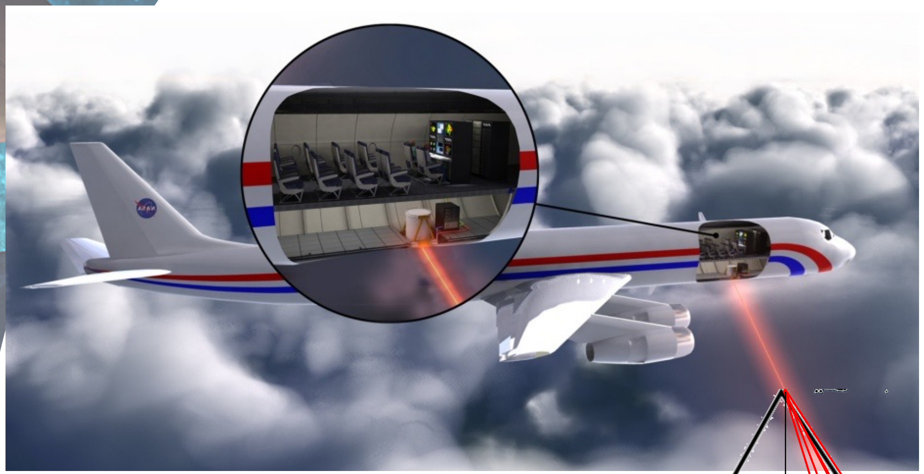

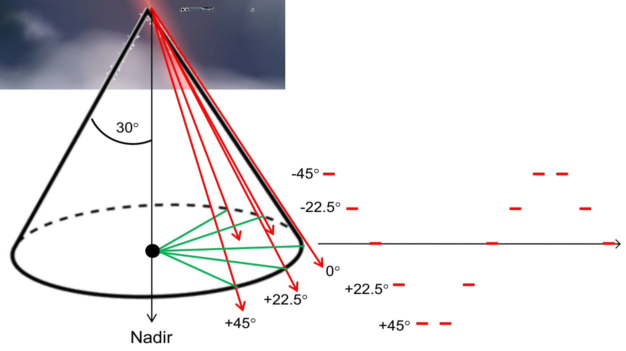

Attribute	Value
Airplanes Flown	DC-8 and UC-12B
Solid-State Laser Crystal and Wavelength	Ho:Tm:LuLiF, 2.053 Microns
Laser Architecture	Master Oscillator Power Amplifier (MOPA)
Pumping Source, Wavelength, Duration	Laser Diode Arrays (LDA), 792 nm, 1 ms
Laser Pulse Energy E, Rate f, FWHM Duration t	80-100 mJ, 10 Hz, 180 ns
Telescope Diameter D	15 cm
Light Detection Material, Technique	InGaAs, Coherent, Dual-Balanced
Scanner Diameter, Type, Deflection	15 cm, Step-Stare Rotating Wedge, 30° About Nadir
Eye Safety	Safe at any Range When DAWN Closed Up for Flight
Pointing Knowledge Technique	Dedicated INS/GPS on Lidar; dry land returns
LOS Wind Measurement Precision	< 1 m/s
Vertical Resolution	60 m

Precision = < 1 m/s

DAWN Capabilities

- 2.053 micron wavelength, 80-100 mJ/pulse. High sensitivity to aerosol backscatter, enables excellent vertical resolution, accuracy, and atmospheric coverage
- Provides vertical profiles of LOS wind, horizontal wind vectors, and aerosol backscatter
- Optional number of azimuth angles (up to 12) permits trade of wind variability determination vs. horizontal resolution
- Optional number of laser shots averaged for each LOS wind profile permits trade of atmospheric coverage vs. horizontal resolution
- Data may be processed multiple ways to provide various combinations of vertical and horizontal resolution, atmospheric coverage, and accuracy
- Successful field campaigns: Polar Winds I and II, Convective Processes Experiment (CPEX), ADM Aeolus Cal/Val Test Flight Campaign